Thin Solid Films 583 (2015) 212–220

Contents lists available at ScienceDirect

Thin Solid Films

journal homepage: www.elsevier.com/locate/tsf

Determination of structural, mechanical and corrosion properties of titanium alloy surface covered by hybrid system based on graphene monolayer and silicon nitride thin films

M. Kalisz [a,*], M. Grobelny [a], M. Zdrojek [b], M. Świniarski [b], J. Judek [b]

[a] Motor Transport Institute, Centre for Material Testing, Jagiellonska 80, Str., Warsaw, Poland
[b] Faculty of Physics, Warsaw University of Technology, Koszykowa 75, 00-662 Warsaw, Poland

ARTICLE INFO

Article history:
Received 10 January 2015
Received in revised form 30 March 2015
Accepted 1 April 2015
Available online 9 April 2015

Keywords:
Silicon nitride thin film
Nanoindentation
Electrochemical properties
Graphene
Graphene hybrid system

ABSTRACT

We report the comparative studies on structural, mechanical and corrosion properties of SiN, SiN/graphene and graphene/SiN hybrid systems deposited on titanium alloy surface.
The deposited silicon nitride thin film and silicon nitride/graphene coatings systems were crack free and exhibited good adherence to the substrate and the surface morphology was homogeneous. The graphene/silicon nitride coating system demonstrated a tendency to peeling off and had poor adhesion to the graphene monolayer deposited on the titanium alloy surface. Graphene transferred on titanium alloy surface and silicon nitride thin film surface was a single layer without defects.
The hardness for silicon nitride thin film and SiN/graphene coatings was the same (22.4 GPa). Graphene coating has no effect on surface hardness but it decreases the electrochemical activity of the system.
The best corrosion resistance has the Ti6Al4V sample coated with SiN/graphene coating system. This sample retains the most stable mechanical and structural parameters during corrosion process. The SiN/graphene coating system greatly improves the mechanical and corrosion properties of examined titanium alloy surface.

1. Introduction

Recently, a significant increase in the world-wide production of castings from light metal alloys such as titanium has been observed. It is related to not only an increase in the demand for lightweight structural components in the automotive, aviation and aerospace industry, but also to an increasing interest from manufacturers of various household appliances, electronics, video cameras, mobile phones and others. The particularly rapid growth in the production of castings from titanium alloys is observed in Germany, Italy and the USA. Wide application of titanium and its alloys is due to their excellent mechanical properties i.e. small specific gravity, yield strength and the modulus of elasticity allowing to the transfer of heavy loads, excellent corrosion resistance and the biocompatibility [1]. The outstanding corrosion resistance of titanium in various test solutions and physiological media is due to the formation of protective oxide layer (TiO_2) on its surface [2]. The oxide layer provides a barrier between the surrounding environment and the underlying metallic titanium what inhibits the subsequent oxidation of metallic titanium across the metal–oxide barrier layer–solution interfaces [3].

Titanium and its alloys have many potential industrial applications, but their implementation is limited due to problems with unsatisfactory surface mechanical parameters, i.e. low hardness, low wear resistance and low corrosion resistance in hot, concentrated and low pH solutions [4–8]. Therefore, many various surface treatment techniques are used, to improve mechanical properties of titanium and its alloys. These methods include burnishing, surface micro-shot peening and thermochemical treatment, in particular based on the physical vapor deposition (PVD) and chemical vapor deposition (CVD) methods [9–11].

One way to protect titanium alloy surface from corrosion and improve its mechanical properties is the application of ceramics coatings i.e. silicon nitride. This leads to the metal's insulation from environmental stress by the unbreakable, durable, elastic and at the same time wear resistance and harder than titanium alloy surface, nitride films [12]. Silicon nitride thin films are characterized by high density, low wear rates, good insulating properties, excellent Na+ resistance, relatively high fracture toughness, strength, high temperature corrosion resistance in oxidizing atmosphere and in sulphidizing–oxidizing atmosphere [13] and excellent biocompatibility [14–17]. They provide an excellent diffusion barrier against water and aggressive contaminants which may corrode titanium alloys [18]. Silicon nitride films can be deposited by low-pressure-chemical-vapor-deposition (LPCVD), plasma enhanced chemical vapor deposition (PECVD) or reactive radio frequency (r.f.) sputtering techniques. Unfortunately, their structural,

* Corresponding author. Tel.: +48 22 43 85 537.
E-mail address: malgorzata.kalisz@its.waw.pl (M. Kalisz).

http://dx.doi.org/10.1016/j.tsf.2015.04.005
0040-6090/

mechanical and corrosion properties highly depend on technological process used during sample fabrication and processing [19–21]. Olofsson et al. in [19] used reactive radio frequency sputtering to produce Si_xN_y coating that showed a potential for high wear resistance, but issues with coating defects and poor adhesion (leading to peeling off of the coating) were reported. Shi et al. in [20] also used different magnetron sputtering methods for fabricating Si_xN_y coating: r.f., direct current and unbalanced magnetron sputtering. However, adhesive properties of the coating were not discussed.

Another way to improve titanium alloys surface properties can be the use of graphene as a protective layer. The studies have shown that a single graphene layer considerably increases the corrosion resistance of such systems as copper/graphene [22], nickel/graphene [23] and titanium alloy/graphene [24] and protects the surface of those metals from oxidation [24].

The purpose of this manuscript is to show that hybrid coating systems based on silicon nitride thin films and graphene monolayer can be used for protection of titanium alloy surface against corrosion process and for improving its surface mechanical properties. In this work, surface, structural, mechanical and corrosion properties of two different hybrid systems: SiN/graphene/Ti–Al–V and graphene/SiN/Ti–Al–V have been investigated and compared with pure titanium alloy and SiN/Ti–Al–V system.

2. Materials and methods

2.1. Sample preparation

2.1.1. Specimen preparation

For the purpose of the experiment, three sets of titanium alloys Ti6Al4V (ASTM Grade 5, UNS R56400, Table 1) were prepared in the same manner. Before technological processes, the Ti alloy surfaces were polished using a grinding and polishing apparatus (Stuers RotoPol 21). The sample surfaces were polished to a "mirror image" and then, the samples were cleaned in an acetone solution.

2.1.2. The silicon nitride thin films preparation

The amorphous silicon nitrides thin films were fabricated in Oxford Plasma Technology PlasmaLab 80 Plus System, which is a parallel plate PECVD (13.56 MHz) deposition system. The computer system allows predefining of the process parameter values and their real-time control during the process. The films prepared by PECVD method have a lot of advantages, such as low deposition temperature, high growth rate, good uniformity and good adhesion to the substrate surface [25].

In order to achieve a range in composition of the SiN films, process parameters such as the deposition pressure, flow rates of SiH_4 and NH_3, the deposition temperature and total gas flow rate were kept constant. Table 2 shows the summary of the parameters used for the deposition of SiN films in this study.

2.1.3. Graphene layer preparation

The graphene monolayers were grown on 18-μm thick copper foil using chemical vapor deposition technique. For this purpose a homemade CVD set based on a Blue M Tube Furnace with a 1-inch diameter reactor tube was used. During the growth process in hydrogen atmosphere, the pressure in the reactor chamber is kept at about ~10^{-6} Torr and temperature is equal to ~1000 °C. Methane is used as a carbon source and the typical growth time is 10 min.

Table 1
Composition of Ti6Al4V titanium alloy.

Components, wt.%						
C	Fe	N	O	Al	V	Ti
0.08	0.25	0.05	0.20	5.50–6.75	3.5–4.5	Bal

Table 2
Summary of the Si_xN_y process parameters.

RF power [W]	120
Pressure [Torr]	0.8
SiH_4 gas flow [ml/min]	150
NH_3 gas flow [ml/min]	50
Temperature [°C]	350

Graphene was transferred on titanium alloy surface and silicon nitride surface using "PMMA-mediated" method [26]. First, PMMA (495 K, about 100 nm thick) was spin-coated on top of the synthesized graphene on copper substrate and dried for 24 h at room temperature. Next, the graphene from bottom of Cu substrate was etched by reactive ion etching method in oxygen plasma (PlasmaLab 80+, Oxford Instruments). After that, the exposed Cu foil was dissolved in an aqueous etchant of iron (III) nitrate for several hours. When the copper was dissolved, the PMMA/graphene sample was cleaned in deionized water. Next, ion particle removing step was used with hydrochloric acid solution, hydrogen peroxide as catalyst dissolved in water [26]. After all cleaning steps PMMA/graphene layer was transferred on the examined surfaces and annealed in order to evaporate water and increase adhesion between graphene and the surface. In the last step the PMMA layer was removed.

2.1.4. Test sample preparation

In Fig. 1 schematic procedures of the test samples preparation are shown.

2.2. Analysis of surface characteristics

The quality and the number of transferred graphene layers graphene were evaluated by Raman spectroscopy (InVia Renishaw Spectrometer, 514 nm laser line, standard mode). All Raman spectra were collected at room temperature using 1 mW laser power (on the sample).

Raman spectroscopy is a nondestructive and fast method for analyzing physical properties of various carbon materials. In case of graphene, Raman spectra give information about number of layers [27], material quality and defects [28]. Typical Raman spectrum of graphene consists of 3 main modes: D mode (~1350 cm^{-1}), G mode (~1580 cm^{-1}) and 2D mode (~2700 cm^{-1}). A monolayer graphene sheet is easily identified by Raman study simply by looking at the G/2D relative intensity ratio (usually about 0.2), also taking into account the shape of those peaks [27]. The quality and defectiveness of a graphene sheet can be verified by the appearance of D mode peak and the ratio of D and G mode intensities [29,30].

The thickness of the deposited hybrid systems was measured by Taylor Hobson Talysurf CCI Lite optical profilometer and was equal to 210 nm.

The elemental composition and the surface morphology of the silicon nitride coatings were investigated with the aid of a Zeiss FE-SEM Merlin with EDS Quantax System (Bruker) scanning electron microscope.

To determine the surface topography properties, atomic force microscopy (AFM) measurements were made by the MultiMode 8 AFM microscope (Bruker) with Peak Force Tapping mode.

2.3. Mechanical characterization

The hardness measurements of the obtained coatings were performed by a nanoindenter manufactured by CSM Instruments equipped with a diamond Vickers indenter. The hardness was calculated using the method proposed by Oliver and Pharr [31]. Each data point represents an average of five indentations. A number of measurements were carried out for various depths of nanoindentation (from 80 nm to 700 nm). In order to measure the "film-only" properties and minimize

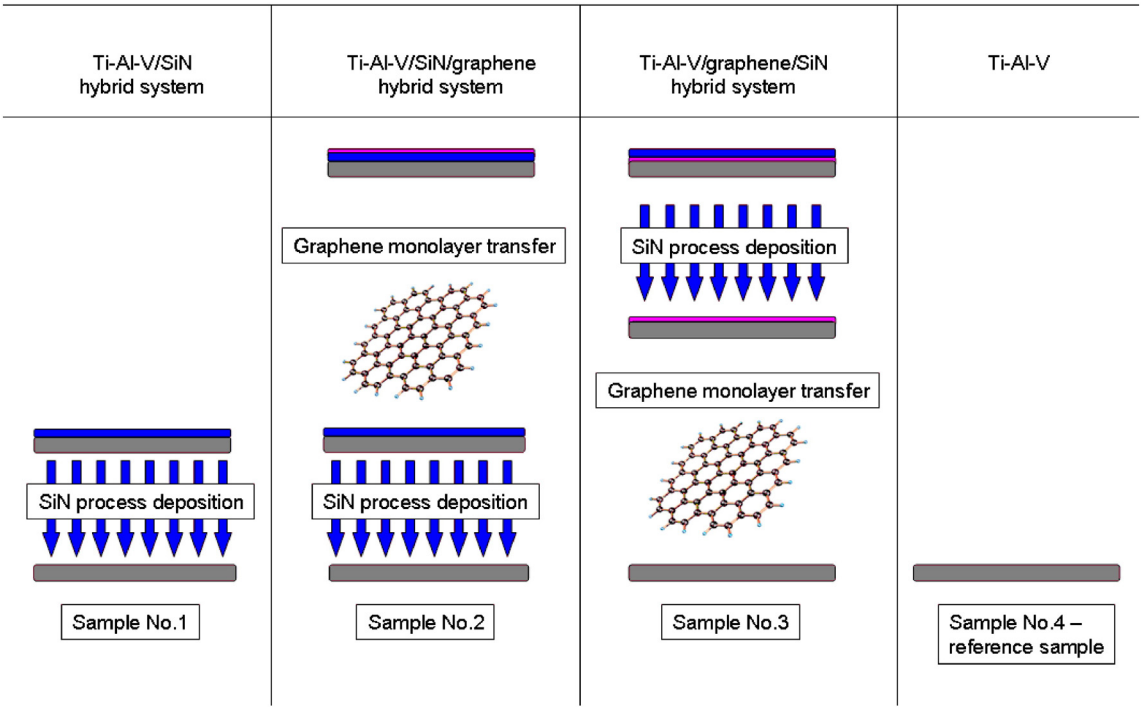

Fig. 1. Schematic procedure of the test sample preparation.

the impact of the substrate, a method of nanoindentation measurements approximation was implemented [32].

2.4. Electrochemical measurements

Electrochemical measurements were carried out in the solution 0.5 M/l NaCl, 2 g/l KF, pH = 2 adjusted by concentrated hydrochloric acid. This solution is characterized by a high corrosivity compared to titanium alloys. It is a more aggressive environment than that of typical electrolytes used for corrosion tests (e.g. artificial saliva, simulated body fluids (SBF)). The voltammetric measurements (polarization curves) were carried out at a scan rate of 1 mV/s within the range of −150 mV to 1000 mV versus open circuit potentials, and polarization curves corresponding to all examined material were recorded. Prior to each polarization experiment, the samples were immersed in the electrolyte for 1 h while monitoring open circuit potential to establish steady state conditions. Each electrochemical measurement for the given material was repeated three times. In the paper we show the most representative results but the differences between the successive values of the open circuit potential (for the same material) did not exceed 50 mV. A three-electrode cell arrangement was applied using the Ag/AgCl electrode with a Luggin capillary as reference electrode and a platinum wire as the auxiliary electrode (counter electrode). The exposed area of the working electrode was 0.2826 cm^2. The measurements were carried out in aerated solutions in room temperature by means of an Autolab EcoChemie System of the AUTOLAB PGSTAT 302 N type equipped with GPESv. 4.9. software. The values of corrosion current densities (i_{corr}) were obtained from the polarization curves by extrapolation of the cathodic and anodic branch of the polarization curves to the corrosion potential [33].

3. Results and discussion

3.1. Potentiodynamic tests

Fig. 2a and b shows open cell potential (OCP) and polarization curves of titanium alloy and titanium alloys with coating system in

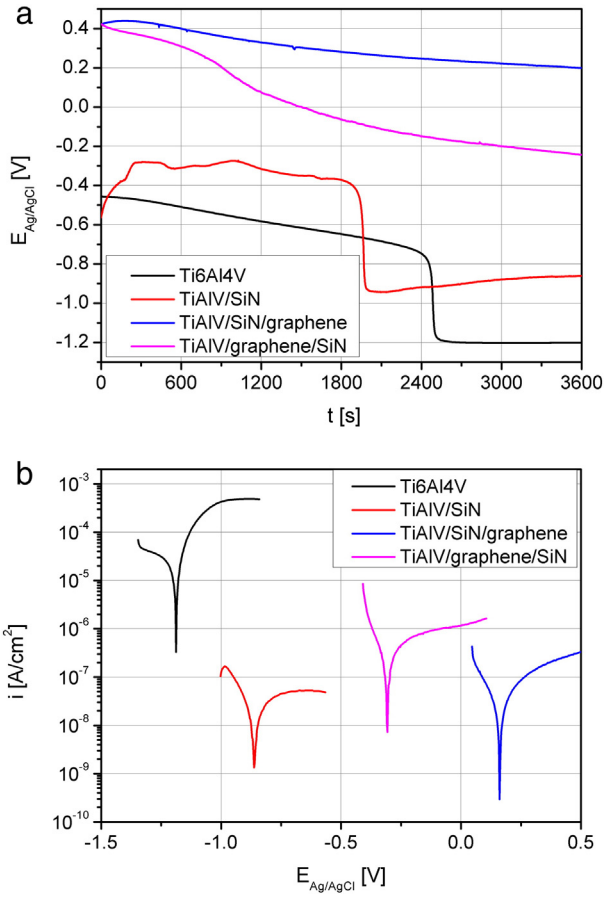

Fig. 2. Open circuit potential (OCP) (a) and polarization curves (b) of Ti6Al4V titanium alloy and titanium alloy with coating system.

0.5 M/l NaCl, 2 g/l KF, pH = 2 electrolyte solution. The results of measurements of electrochemical parameters of the samples obtained from polarization curves are collected in Table 3.

In the case of titanium alloy with coatings, one can observe a significant improvement in the corrosion properties what is reflected in the decrease of corrosion current density i_{corr} and shift of corrosion potential E_{corr} values to the noble potentials. The smallest value of i_{corr} and the best corrosion properties were obtained for the Ti6Al4V/SiN and TiAlV/SiN/graphene coatings systems. However, corrosion potential value for the TiAlV/SiN/graphene coatings system was $E_{corr} = 0.162$ V, which is much more positive than E_{corr} registered for the other samples. A positive value of the corrosion potential is characteristic for materials with low electrochemical activity and thereby very good corrosion resistance. It should also be noted that the course of potential is very stable. During 1 h exposure, the potential changed only by about 200 mV. For the sample covered by the SiN thin film despite the low value of i_{corr}, a much more negative corrosion potential was observed. During exposure in the electrolyte solution, after about 1800 s a sharp decline in the value of the potential (from −0.4 V to −0.9 V) takes place. This is probably due to the penetration of the coating by the electrolyte and the corrosive reaction of titanium alloy. Similar course of OCP for titanium alloy without coating was observed. In this case after about 2400 s a sharp decline in the value of the potential (from −0.75 V to −1.20 V) takes place. However, this change is caused by the damage of the oxide layer present on the surface of a titanium alloy. The oxide layer acts a barrier and protection against general corrosion processes. However, in the environment of acidic pH (pH ca. 2) the protective layer is unstable and the processes of corrosion of metallic Ti or its alloys are initiated. This phenomenon is accelerated in the presence of aggressive ions such as fluoride ions [34–37].

For the SiN/graphene coating system on Ti alloy indirect corrosion properties was observed. The value of corrosion current density obtained for TiAlV/graphene/SiN coatings system is higher than the values obtained for the TiAlV/SiN and TiAlV/SiN/graphene coatings systems. This is probably due to the poor quality of silicon nitride thin film.

The value of the corrosion potential is located between values obtained for the TiAlV/SiN and TiAlV/SiN/graphene coatings systems. The more positive value of the corrosion potential than E_{corr} obtained for the TiAlV/SiN is due to the presence of the graphene layer at the structure interface, which prevents the electrolyte from interacting with the titanium alloy. However, more negative value of this parameter than the value obtained for coating system with graphene monolayer on the top is probably due to the poorer quality of the graphene monolayer, than in the case of TiAlV/SiN/graphene coatings system. It should also be noted that the course of potential for the TiAlV/graphene/SiN coatings system is quite stable. During 1 h exposure the potential changed only by about 600 mV.

3.2. Structural characterization

SEM images of the surfaces of the investigated coatings before and after being subjected to the corrosion tests are shown in Fig. 3a–f. The SEM images reveal the interesting differences between the samples depending on their composition. SiN thin film (sample no. 1) and SiN/graphene (sample no. 2) were crack free, exhibited good adherence to the substrate and no discontinuities in the surface morphology were observed (see Fig. 3a and c, respectively).

Completely different results were obtained for the TiAlV/graphene/SiN coatings system (sample no. 3). The silicon nitride thin film deposited on the top of the graphene monolayer was peeled off what suggests poor adhesion of the SiN thin film to the graphene surface (Fig. 3e).

After corrosion process, only SiN/graphene sample presents almost no changes (Fig. 3d) with respect to the samples no. 1 (Fig. 3b) and no. 3 (Fig. 3f). Deposition of the graphene monolayer on the top of the silicon nitride thin film causes that after the corrosion test the dendritic structures on the surface of the coating system are formed (see Fig. 3d). However, the layer is still crack free and densely packed.

The different results were obtained for the sample no. 1 (silicon nitride thin film). After the corrosion process, the clearly visible holes appeared in the structure of the SiN film (Fig. 3b). This is probably due to the penetration of the coating by the electrolyte, whereby the the layer is degraded.

In the case of the sample no. 3 (Fig. 3f), an introduction of the graphene monolayer causes cracking and detachment of the silicon nitride thin film, during corrosion process. These damages to the SiN layer could be responsible for the decline in value of the corrosion current density i_{corr} (see Table 3 and Fig. 2b) for the TiAlV/graphene/silicon nitride coatings system.

The results of X-ray microanalysis showed that, the places where silicon nitride thin film fell off, consist of titanium, aluminum, vanadium (which are the components of used titanium alloy), carbon (coming probably from graphene layer) and oxide—the corrosion product of titanium alloy substrate (Fig. 4a). The thin film remaining on the sample surface after corrosion process is composed of the silicon and nitrogen, which are the components of deposited SiN thin film (Fig. 4b). Interestingly, the morphology of the remained silicon nitride thin film, viewed in the magnification 25 k, is not smooth and looks like “orange peel” (see Fig. 5) [38].

For further information about the surface topography of the selected coatings systems after corrosion process, the AFM measurements were performed.

In Fig. 6 the two-dimensional AFM image for silicon nitride/graphene coatings system (sample 2) is shown. It is clearly seen, that after corrosion process (Fig. 6a), the regions in the gaps changed color (white), thus it indicates that in these regions oxide layer was formed [39] (see Fig. 6a). During the SEM measurements the oxidized regions in the gaps look like “dendritic”. The silicon nitride regions under the graphene flakes are still pristine what indicates that these regions are not oxidized [39]. The silicon nitride regions located under graphene flakes are better protected than regions located under the gaps. The surface of silicon nitride/graphene coatings system, after corrosion process is still crack free and densely packed. For comparison, in Fig. 6b is shown a two dimensional AFM image of the silicon nitride/graphene coatings system, before corrosion process.

As in the case of SEM measurements (as shown in Fig. 3c), the AFM measurements showed no cracks and no discontinuity for the graphene monolayer deposited on silicon nitride surface. The surface of graphene was flat and homogenous. The silicon nitride thin film under the graphene layer was pristine and shiny, which indicated that silicon nitride thin film was not oxidized [39].

In Fig. 6c the AFM image of the graphene/SiN coatings system, after corrosion process is shown. The thin film remaining on the surface is densely packed and most of the boundaries between adjacent grains in the silicon nitride is “sealed” [40]. It seems that the top layer of the graphene/SiN coating system is composed of many big particles with quite regular shapes, with the height about 85 nm. During the SEM measurements these particles may resemble the “orange peel”.

Table 3
Corrosion tests results of Ti6Al4V alloy and Ti6Al4V alloy with coating system obtained from polarization curves in 0.5 M NaCl, pH = 2, 2 g/l KF solution.

Sample	i_{corr} [A/cm^2]	E_{corr} [V]
TiAlV/SiN	5.8E − 08	−0.866
TiAlV/SiN/graphene	5.1E − 08	0.162
TiAlV/graphene/SiN	4.5E − 07	−0.307
Ti6Al4V	6.1E − 05	−1.188

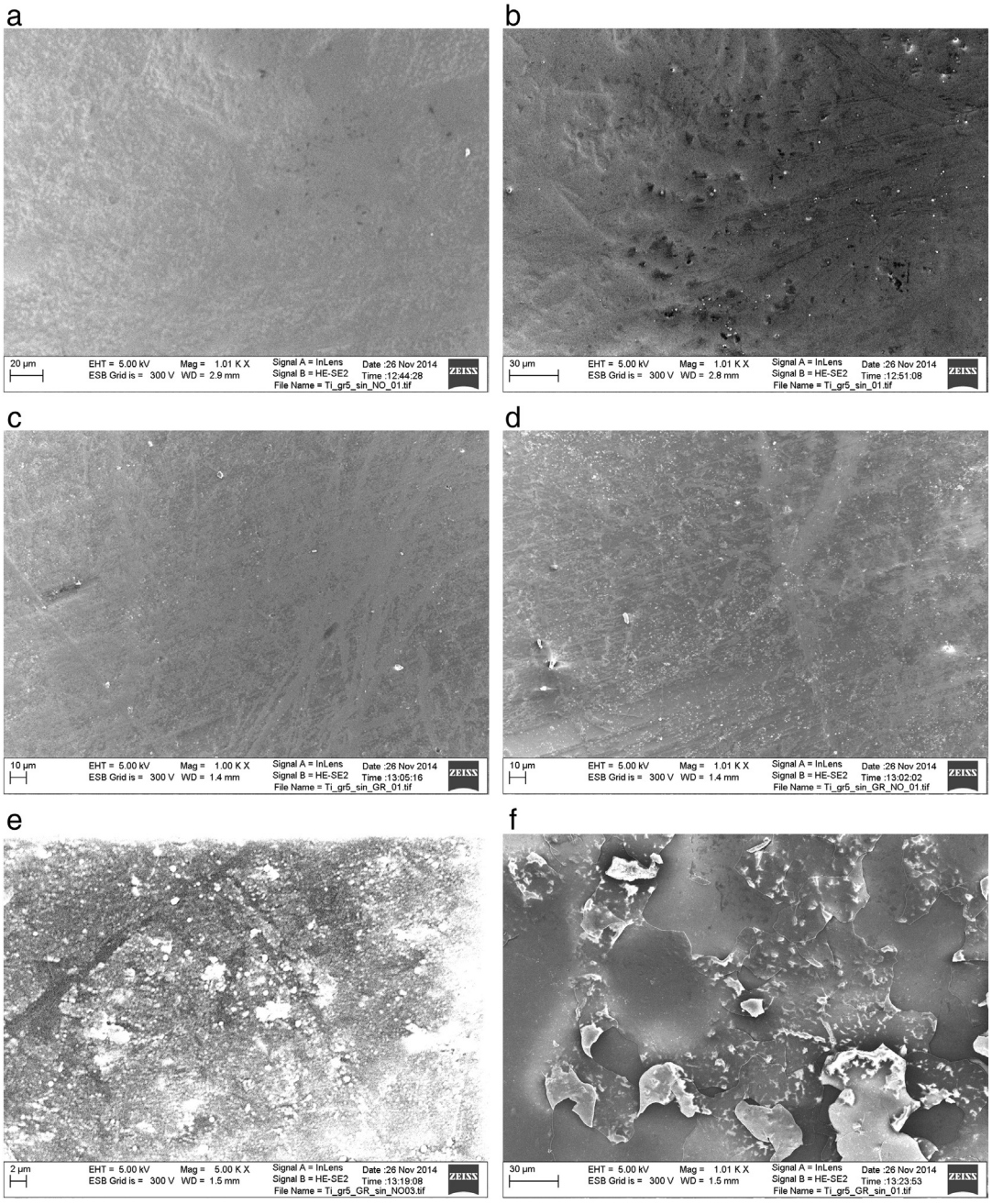

Fig. 3. SEM images of as-deposited hybrid systems: a) SiN before corrosion process, b) SiN after corrosion process, c) SiN/graphene before corrosion process, d) SiN/graphene after corrosion process, e) graphene/SiN before corrosion process and f) graphene/SiN after corrosion process.

3.3. Raman characterization

Fig. 7 shows the comparison of Raman spectra collected before and after corrosion treatment on Ti–Al–V/SiN/graphene system. Despite the corrosion process the Raman signatures of graphene are still present, suggesting that graphene might be a corrosion-resistant layer. The decrease of the intensity of the main modes (about 3 times for G mode) after corrosion treatment might suggest better graphene adhesion with the SiN surface. The relative intensity of I_D/I_G ratio has lower value after corrosion indicating that graphene layer is less defective. The relative intensity ratio IG/I2D modes are lower after corrosion process probably because of cleaning graphene sheet during corrosion measurements. Before corrosion process graphene sheet is doped with contamination that left after transfer process (e.g. Fe^{3+}, $(NO_3)^{3-}$ ions [41] or PMMA residues [42]). Doped graphene characterized with lower intensity of 2D mode (increasing of Fermi energy level [43]) while intensity of G mode is insensitive to the doping [44]. After corrosion treatment most of contamination that left after transfer process are washed out and the intensity of 2D mode increased. Also peak shift indicates the change in doping level before and after corrosion measurement [43], which also suggests removal of some amount of chemical leftover.

For the Ti–Al–V/graphene/SiN system we first verified Raman spectra for graphene layer before deposition of SiN (Fig. 8a). The negligible D mode seen on the spectrum suggests that graphene layer is without structural defects. Moreover the intensity ratio of G and 2D modes shows that this is indeed a monolayer graphene (see ref. [27]).

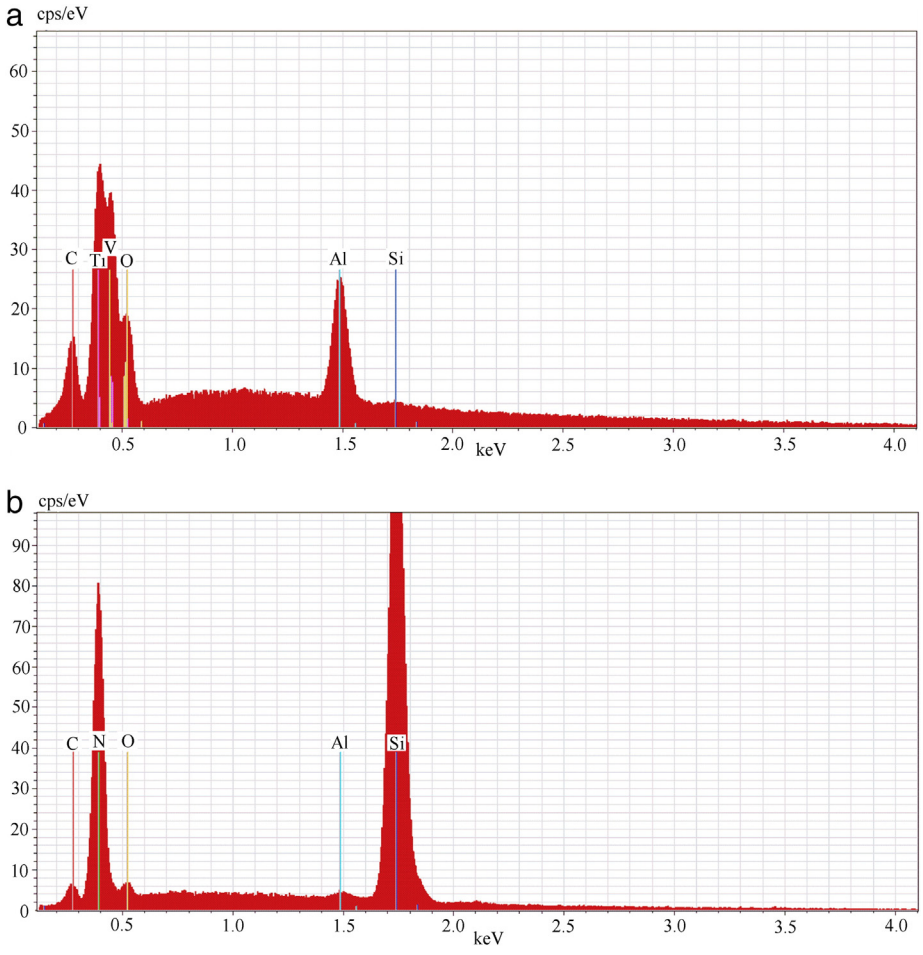

Fig. 4. Results of X-ray microanalysis showing the chemical composition of the area: a) after falling off the layer, and b) of the residue layer, both after corrosion process.

After SiN deposition we found some areas where SiN layer peeled off from graphene surface forming some kind of holes which suggests low silicon nitride adhesion to thin carbon layer. The Raman spectra collected in those peeled off areas show existence of amorphous carbon (Fig. 8b–c) [45]. So, the SiN deposition process seems to strongly deteriorate the quality of deposited graphene, resulting in a shift of the electrochemical potential towards negative values (see Fig. 2b). The inset in Fig. 8b corresponds to the signal collected on SiN layer that was supposed to cover graphene, but this time showing no evidence of carbon. This might be caused by the fact that SiN completely screens the Raman signal of carbon from the underlying layer, especially if this is an amorphous carbon layer which has usually lower intensity than graphene.

The spectra collected in corrosion area exhibit carbon signatures of much lower intensity than before corrosion. This suggests that corrosion treatment removed part of the amorphous carbon layer from the open holes.

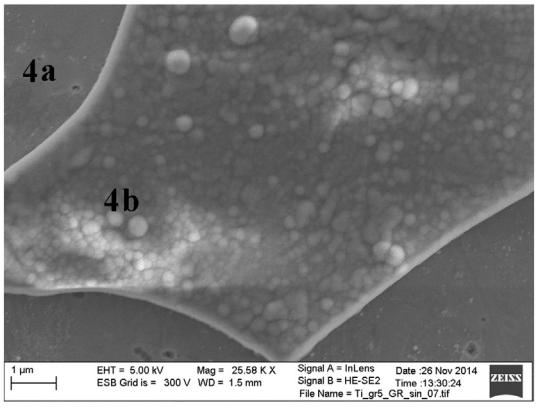

Fig. 5. SEM image of graphene/SiN hybrid system after corrosion process (magnification 25 k).

3.4. Mechanical characterization

The hardness of prepared coatings systems was measured by nanoindentation and determined by an approximation method [32]. For pure titanium alloy nanohardness has been measured at a constant depth equal to 80 nm. It is the smallest depth, for which the correct results have been obtained. Additionally, the root mean square error (RMSE) was calculated.

The hardness obtained for the uncoated titanium alloy (sample no. 4), silicon nitride thin film (sample no. 1), silicon nitride/graphene (sample no. 2) and graphene/silicon nitride (sample no. 3) coatings systems, was equal to (5.94 ± 0.2) GPa, (22.4 ± 0.5) GPa (Fig. 9a), (23.0 ± 0.5) GPa (Fig. 9b) and (22.2 ± 0.5) GPa (Fig. 9c), respectively. As compared to the results presented in the literature reports, hardness of investigated silicon nitride thin films is higher of ca. 51% [38–40,45–47] and 22% [48].

Graphene monolayer deposited on silicon nitride thin film (sample no. 2) is practically not seen by nanoindenter during measurements. Therefore, the measurement did not reveal changes in hardness after graphene deposition, in comparison with the silicon nitride thin film, and was equal (23.0 ± 0.5) GPa (Fig. 9b).

The nanoindentation measurements, performed after the corrosion process, show no change of surface hardness for sample no. 2.

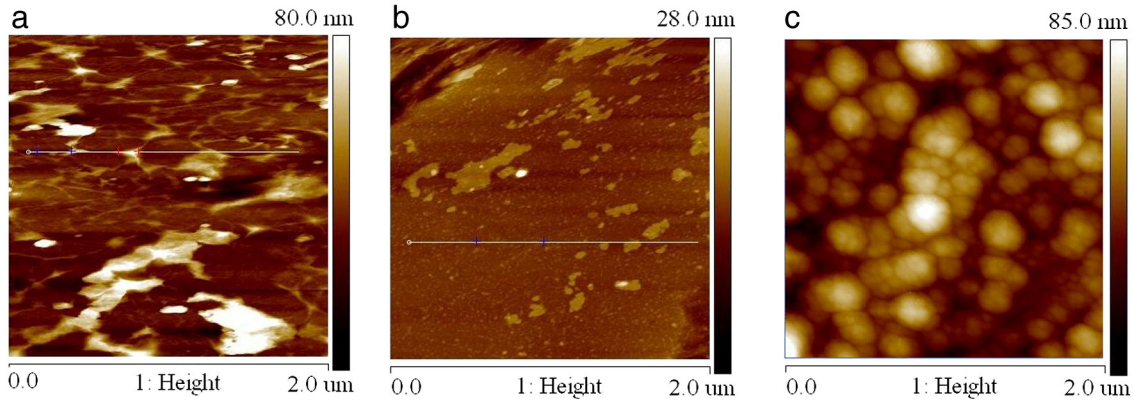

Fig. 6. AFM image of a) deposited SiN/graphene coating system after corrosion process, b) deposited SiN/graphene coating system before corrosion process and c) graphene/SiN coating system remained on the substrate after corrosion process.

In the case of the sample no. 1 and the sample no. 3, a decrease of surface hardness is observed. The hardness obtained for the silicon nitride thin film was equal (13.9 ± 0.5) GPa (Fig. 9a) and for the graphene/silicon nitride coatings system: (20.6 ± 0.5) GPa (Fig. 9c) The value of surface hardness decreased by 13% for silicon nitride thin film and by 7% for graphene/silicon nitride coatings system as compared to the value obtained for the same layers before corrosion process and titanium alloy before and after corrosion process. The hardness of titanium alloy surface before the corrosion process was equal to (5.94 ± 0.2) GPa and after corrosion process: (4.95 ± 0.2) GPa.

In the case of uncoated silicon nitride thin film, decreasing of surface nanohardness after corrosion process can be caused by corrosion degradation of the layer and titanium alloy surface under it [24].

As can be seen from nanoindentation measurements (Fig. 9c), the changes observed on the surface of the sample no. 3 (influenced by corrosion process, i.e. cracks and detachment of the layer) did not have a significant effect on the change of the nanohardness value of this coatings system. Deposition of the graphene monolayer on the titanium alloy surface before silicon nitride thin film formation, reduces degradation processes of the film during corrosion process, which takes place in case of the coating system without graphene monolayer (TiAlV/SiN coating system).

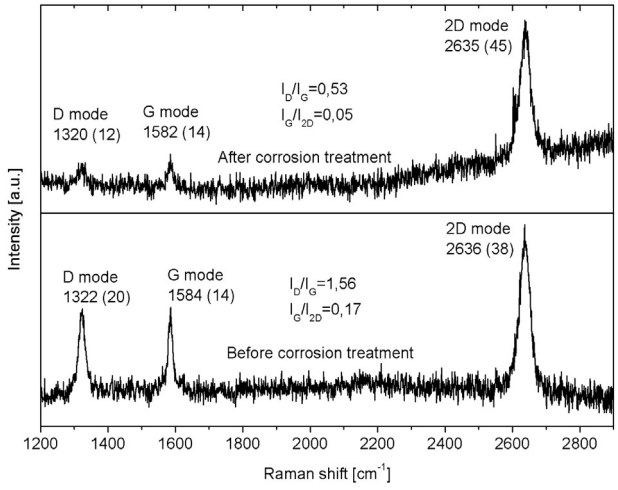

Fig. 7. Typical Raman spectra before and after corrosion process of Ti–Al–V/SiN/graphene system. Both spectra were collected using the same measurement parameters (633 nm laser line, 60 s of exposure time and two accumulations).

4. Summary

We have shown that SiN thin film, SiN/graphene and graphene/SiN coating systems deposited on titanium alloy surfaces, can be considered as coatings that improve surface hardness of a Ti6Al4V alloy.

Among all three tested coating systems, only the TiAlV/SiN/graphene and TiAlV/graphene/SiN systems can be considered as barrier

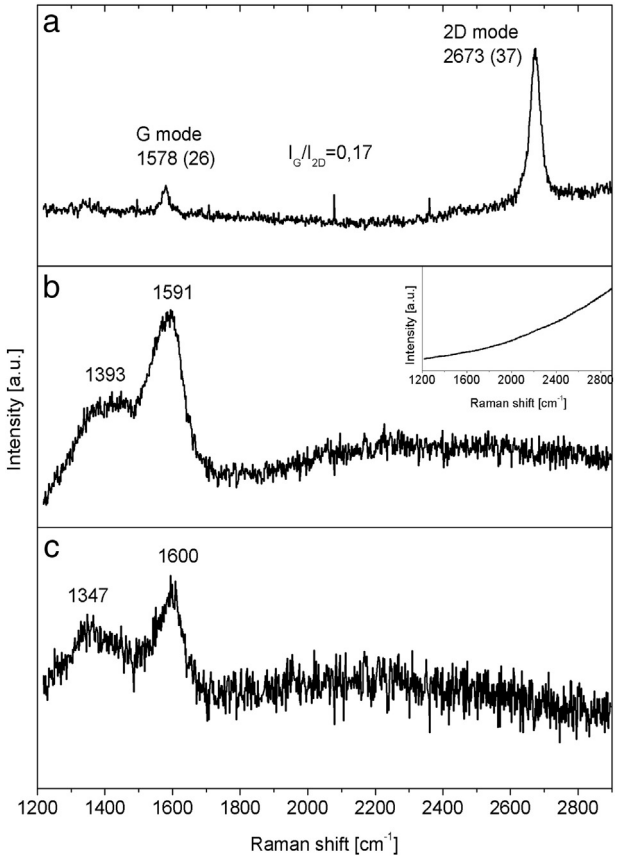

Fig. 8. Raman spectra of Ti–Al–V/graphene system (A), Ti–Al–V/graphene/SiN system before(B) and after (C) corrosion process. The inset graph (B) shows typical Raman spectra of SiN coating graphene in the range of 1200–2900 cm^{-1}. SiN spectra look similar for both before and after corrosion. All Raman spectra were collected using the same measurements parameters (514 nm laser line, 30 s of exposure time and one accumulation).

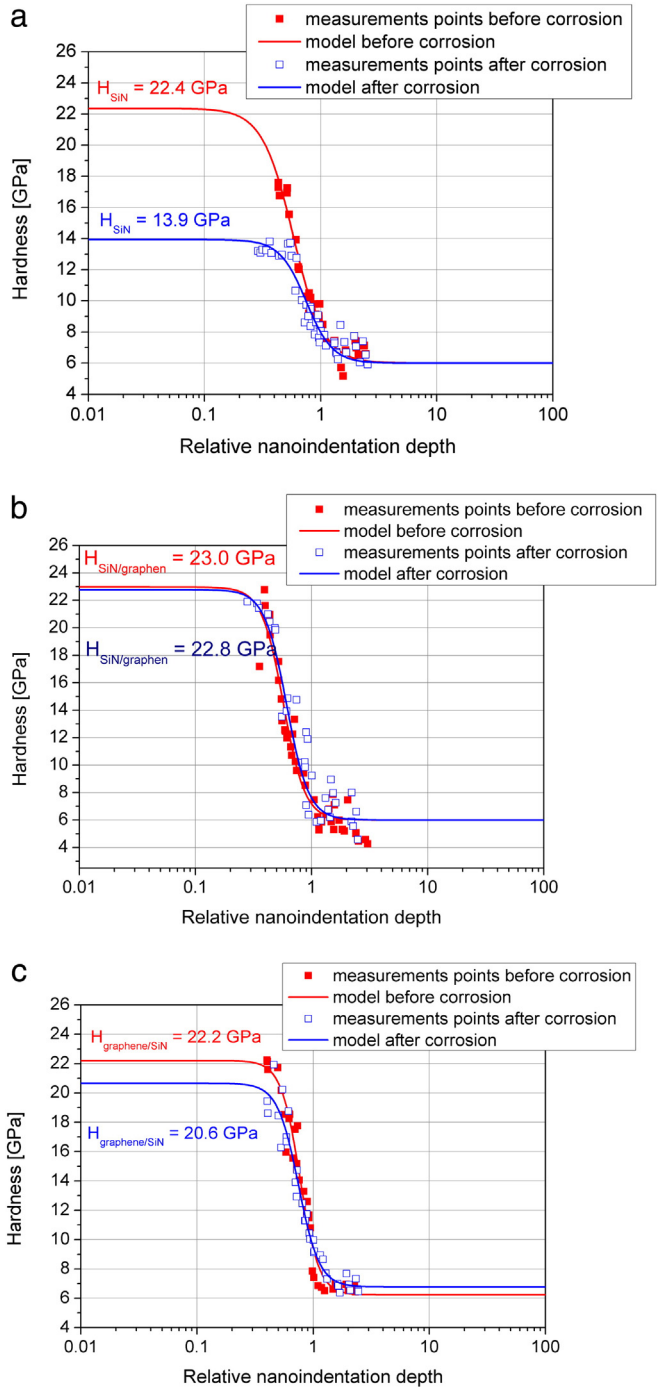

Fig. 9. Results of hardness investigation for a) SiN thin film, b) SiN/graphene coatings system and c) graphene/SiN coatings system, before and after corrosion process.

coatings systems for the Ti6Al4V alloy. They protect its surface against corrosion processes which take place on pure titanium alloy surface in very aggressive environments. Moreover, these coating systems maintain stability of the mechanical properties during corrosion process. Instead, only for the silicon nitride/graphene coating system is not observed structural degradation during corrosion process.

In the next step, the investigations on resistance to corrosion and mechanical properties of hybrid systems during temporary exposure to corrosive environments (artificial saliva, SBF etc.) will be performed.

Acknowledgments

This work was funded by the National Centre for Research and Development in the years 2013–1016 as a research project no. GRAFTECH/NCBR/14/26/2013 “InGrafTi”.

References

[1] K. Elagli, M. Traisnel, H.F. Hildebrand, Electrochemical behaviour of titanium and dental alloys in artificial saliva, Electrochim. Acta 38 (1993) 1769.
[2] M. Al-Mayouf, A.A. Al-Swayih, N.A. Al-Mobarak, Effect of potential on the corrosion behavior of a new titanium alloy for dental implant applications in fluoride media, Mater. Corros. 55 (2004) 88.
[3] R. Goldberg, J.L. Gilbert, The electrochemical and mechanical behavior of passivated and TiN/AlN-coated CoCrMo and Ti6Al4V alloys, Biomaterials 25 (5) (2004) 851.
[4] C.P. Dillon, Phorgotten phenomena: behavior of reactive metals, Mater. Perform. 7 (1998) 69.
[5] R. Strietzel, A. Hosch, In vitro corrosion of titanium, Biomaterials 19 (1998) 1495.
[6] R.W. Schutz, D.E. Thomas, Corrosion of titanium and titanium alloys, Metals handbook, 9th ed., 13, Metals Park, OH: American Society for Metal (ASM) International 1987, p. 669.
[7] R.W. Schutz, D.E. Thomas, Corrosion of titanium and titanium alloys, Metals Handbook, 9th ed., 13, Metals Park International American Society for Metal (ASM) 1987, p. 669.
[8] L. Kinani, A. Chtaini, Corrosion inhibition of titanium in artificial saliva containing fluoride, Leonardo J. Sci. 12 (11) (2007) 33.
[9] Y. Song, Z. Zhao, F. Lu, Experimental study of the influence of shot peening on the microstructure and properties of surface layer of a TC21 titanium alloy atlas, J. Mater. Sci. 1 (1) (2014) 17.
[10] S. Thamizhmnaii, B. Bin Omar, S. Saparudin, S. Hasan, Surface roughness investigation and hardness by burnishing on titanium alloy, J. Achiev. Mater. Manuf. Eng. 28 (2) (2008) 139.
[11] K.-T. Rie, Th. Lampe, Thermochemical surface treatment of titanium and titanium alloy Ti6Al4V by low energy nitrogen ion bombardment, Mater. Sci. Eng. 69 (2) (1985) 473.
[12] X. Liua, P.K. Chub, Ch. Dinga, Surface modification of titanium, titanium alloys, and related materials for biomedical applications, Mater. Sci. Eng. R 47 (2004) 49.
[13] J. Pitter, J. Cizner, F. Černý, M.A. Djouadi, A. Koutsomichalis, The influence of gradient SiNx IBAD coating on corrosion resistance of alloy steels in oxidizing and sulphidizing–oxidizing atmosphere at high temperature, Surf. Coat. Technol. 90 (1998) 1169.
[14] M. Mazzocchi, A. Bellosi, On the possibility of silicon nitride as a ceramic for structural orthopedic implants. Part I: processsing, microstructure, mechanical properties, cytotoxicity, J. Mater. Sci. Med. 19 (8) (2008) 2881.
[15] M. Mazzocchi, D. Gardini, P. Luigi Traverso, M. Giulia Faga, A. Bellosi, On the possibility of silicon nitride as a ceramics for structural orthopaedic implants. Part II: chemical stability and wear resistance in body environment, J. Mater. Sci. Med. 19 (8) (2008) 2889.
[16] S.B. Bal, A. Khandkar, R. Lakshminarayanan, I. Clarke, A.A. Hoffman, M.N. Rahaman, Testing of silicon nitride ceramic bearings for total hip arthroplasty, J. Biomed. Mater. Res. B Appl. Biomater. 87B (2) (2008) 447.
[17] S.B. Bal, A. Khandkar, R. Lakshminarayanan, I. Clarke, A.A. Hoffman, M.N. Rahaman, Fabrication and testing of silicon nitride bearings in total hip arthroplasty: winner of the 2007 “HAP” PAUL award, J. Arthroplast. 24 (1) (2009) 110.
[18] M-Ch. Joa, S.-K. Park, S.-J. Park, A study on resistance of PECVD silicon nitride thin film to thermal stress-induced cracking, Appl. Surf. Sci. 140 (1999) 12.
[19] J. Olofsson, T. Mikael Grehk, T. Berlind, C. Persson, S. Jacobson, H. Engqvist, Evaluation of silicon nitride as a wear resistant and resorbable alternative for total hip joint replacement, Biomaterials 2 (2) (2012) 94.
[20] Z. Shi, Y. Wang, C. Du, N. Huang, L. Wang, C. Ning, The structure, surface topography and mechanical properties of Si–C–N films fabricated by RF and DC magnetron sputtering, Appl. Surf. Sci. 258 (4) (2011) 1328.
[21] Z. Shi, Y. Wang, C. Du, N. Huang, L. Wang, C. Ning, Silicon nitride films for the protective functional coating: blood compatibility and biomechanical property study, J. Mech. Behav. Biomed. Mater. 16 (2012) 9.
[22] E. Teo, Y. Lih, R. Mat Zaid, T. Ling Ling, K.F. Chong, Facile corrosion protection coating from graphene, Int. J. Chem. Eng. Appl. 3 (6) (2012) 453.
[23] D. Prasai, J.C. Tuberquia, R.R. Harl, G.K. Jennings, K.I. Bolotin, Graphene: corrosion-inhibiting coating, ACS Nano 6 (2012) 1102.
[24] M. Kalisz, M. Grobleny, M. Mazur, D. Wojcieszak, M. Świniarski, M. Zdrojek, J. Domaradzki, D. Kaczmarek, Mechanical and electrochemical properties of Nb2O5, Nb2O5:Cu and graphene layers deposited on titanium alloy (Ti6Al4V), Surface and Coating Technology (2015).
[25] L. Liu, W.-G. Liu, N. Cao, Ch.-L. Cai, Study on the performance of PECVD silicon nitride thin films, Def. Technol. 9 (2013) 121.
[26] X. Liang, B.A. Sperling, I. Calizo, G. Cheng, C.A. Hacker, Q. Zhang, Y. Obeng, K. Yan, H. Peng, Q. Li, X. Zhu, H. Yuan, A.R. Hight Walker, Z. Liu, L. Peng, C.A. Richter, Toward clean and crackless transfer of graphene, ACS Nano 5 (2011) 9144.
[27] A. Jorio, R. Saito, G. Dresselhaus, M.S. Dresselhaus, Raman Spectroscopy in Graphene-Based Systems: Prototypes for Nanoscience and Nanometrology, Wiley-VCH, 2011.
[28] V. Singh, D. Joung, L. Zhai, S. Das, S.I. Khondaker, S. Seal, Graphene based materials: past, present and future, Prog. Mater. Sci. 56 (2011) 1178.
[29] A. Gupta, G. Chen, P. Joshi, S. Tadigadapa, P.C. Eklund, Raman scattering from high-frequency phonons in supported n-graphene layer films, Nano Lett. 6 (2006) 2667.

[30] A.C. Ferrari, J.C. Meyer, V. Scardaci, C. Casiraghi, M. Lazzeri, F. Mauri, S. Piscanec, D. Jiang, K.S. Novoselov, S. Roth, A.K. Geim, Raman spectrum of graphene and graphene layers, Phys. Rev. Lett. 97 (2006) 187401.
[31] W.C. Oliver, G.M. Pharr, An improved technique for determining hardness and elastic modulus using load and displacement sensing indentation experiments, J. Mater. Res. 7 (1992) 1564.
[32] Y.-G. Jung, B.R. Lawn, M. Martyniuk, H. Huang, X.Z. Hu, Evaluation of elastic modulus and hardness of thin films by nanoindentation, J. Mater. Res. 19 (2004) 3076.
[33] F. Mansfeld, Electrochemical methods of corrosion testing, ASM International ASM Handbook13A2003. 446.
[34] G. Boere, Influence of fluoride on titanium in an acidic environment measured by polarization resistance technique, J. Appl. Biomater. 6 (4) (1995) 283.
[35] M. Nakagawa, S. Matsuya, T. Shiraishi, M. Ohta, Effect of fluoride concentration and pH on corrosion behavior of titanium for dental use, J. Dent. Res. 78 (1999) 1568.
[36] R.W. Schutz, D.E. Thomas, Corrosion of titanium and titanium alloys, Metals Handbook, 13, American Society for Metal (ASM) International, Metals Park, OH 1987, p. 669.
[37] L. Kinani, A. Chtaini, Corrosion inhibition of titanium in artificial saliva containing fluoride, Leonardo J. Sci. 6 (11) (2007) 33.
[38] H. Huang, K.J. Winchester, A. Suvorova, R.R. Lawn, Y. Liu, Effect of deposition conditions on mechanical properties of low-temperature PECVD silicon nitride films, Mater. Sci. Eng. A 435–436 (2006) 453.
[39] G. Ramírez, S.E. Rodil, S. Muhl, D. Turcio-Ortega, J.J. Olaya, M. Rivera, E. Camps, L. Escobar- Alarcón, Amorphous niobium oxide thin films, J. Non-Cryst. Solids 356 (50-51) (2010) 2714.
[40] D. Zhu, H.-T. Lin, S. Mathur, T. Ohji, Aluminium Oxide and Silicon Nitride Thin Films as Anticorrosion Layers, Wiley-VCH, 2010.
[41] Y.Y. Wang, P.J. Burke, A large-area and contamination-free graphene transistor for liquid-gated sensing applications, Appl. Phys. Lett. 103 (2013) (052103-1 ÷ 4).
[42] J.W. Suk, A. Kitt, C.W. Magnuson, Y. Hao, S. Ahmed, J. An, A.K. Swan, B.B. Goldberg, R.S. Ruoff, Transfer of CVD-grown monolayer graphene onto arbitrary substrates, ACS Nano 5 (9) (2011) 6916.
[43] A. Das, S. Pisana, B. Chakraborty, S. Piscanec, S.K. Saha, U.V. Waghmare, K.S. Novoselov, H.R. Krishnamurthy, A.K. Geim, A.C. Ferrari, A.K. Sood, Monitoring dopands by Raman scattering in an electrochemically top-gated graphene transistor, Nat. Nanotechnol. 3 (2008) 210.
[44] C. Casiraghi, Doping dependence of the Raman peaks intensity of graphene close to the dirac point, Phys. Rev. B 80 (23) (2009) 233407.
[45] M. Marton, M. Vojs, E. Zdravecká, Raman spectroscopy of amorphous carbon prepared by pulsed arc discharge in various gas mixtures, J. Spectrosc. 2013 (2013) 1.
[46] P.-H. Wua, I.-K. Linc, H.-Y. Yana, K.-S. Oua, K.-S. Chena, X. Zhange, Mechanical property characterization of sputtered and plasma enhanced chemical deposition (PECVD) silicon nitride films after rapid thermal annealing, Sensors Actuators A Phys. 168 (2011) 117.
[47] Z.-K. Huang, K.-Sh. Chen, Nanoindentation fracture and fatigue characterization of PECVD silicon nitride films subjected to rapid thermal annealing, Sensors Actuators A Phys. 207 (2014) 49.
[48] M. Vila, D. Caceres, C. Prieto, Mechanical properties of sputtered silicon nitride thin films, J. Appl. Phys. 94 (2003) 7868.